Materials Research. 2022; 25:e20210556
DOI: https://doi.org/10.1590/1980-5373-MR-2021-0556

Effect of Al_2O_3 in Refining Slag on the Cleanliness and Fatigue Property of Ultra-low-carbon Automotive Steel

***Shujun Li*[a,b], *Xueyan Du*[a,b*]**

[a]*Lanzhou University of Technology, School of Materials Science and Engineering, 730050, Lanzhou, China.*
[b]*Lanzhou University of Technology, State Key Laboratory of Advanced Processing and Recycling of Non-Ferrous Metals, 730050, Lanzhou, China.*

Received: October 28, 2021; Accepted: December 28, 2021.

The influence of Al_2O_3 content in refining slag on the cleanliness and fatigue property of ultra-low-carbon (ULC) automotive steel were investigated based on the industrial experiments. The inclusion-adsorption capacity of the refining slag was calculated and the total [O] (T.O) content of ULC automotive steel was measured. The number density, size distribution and morphology of inclusions were analyzed and their effects on the cleanliness and fatigue property of ultra-low-carbon (ULC) automotive steel were investigated. The results showed that as the Al_2O_3 content in refining slag increased from 19.92% to 39.73%, the inclusion-adsorption capacity of ULC automotive steel decreased from 210.30 down to 57.12, and the fatigue life from $1.4x10^4$ down to $0.9x10^4$ cycles, while the T.O content of steel increased from 12 up to18 ppm and the inclusion number density from 4 up to 9 per mm^2.

Keywords: *refining slag, adsorption capacity, cleanliness, fatigue property, UCL automotive steel.*

1. Introduction

With the rapid development of the automotive industry, methods of improving the quality and performance of steel have attracted significant attention in recent years. The ULC steel, as important candidate steel for the automotive industry, requires high cleanliness to guarantee the appropriate mechanical properties for undergoing subsequent processing and utilization[1].

It is now a clearly investigation that the non-metallic inclusions are usually the resources affecting the cleanliness and fatigue properties in ULC automotive steel. The microvoids and cracks at inclusion/steel interfaces produced by non-metallic inclusions were found to be the resources of fatigue fractures, so the presence of non-metallic inclusions such as Al_2O_3 could decrease the cleanliness and mechanical properties of the steel, especially of fatigue properties[2]. Therefore, how to control non-metallic inclusions at the ultralow level is in the pursuit of ULC automotive steel production[3,4].

The investigation of the cleanliness of ULC automotive steel indicated that an appropriate refining slag caused the inclusions to be removed effectively from steel, resulting in the improvement of the cleanliness and the mechanical properties of the steel. Since the slag in the refining process could control and remove inclusions from the molten steel effectively[5], slag systems and models were designed to investigate the influence of the mechanical properties[6-8]. The improved methods for controlling inclusions have thus been reported[9-12]. When the Al_2O_3 content in the refining slag increased from 14.71% to 22.3%, the number density of inclusions increased from 5.2 to 6.5 and the largest size of inclusion raised from 7.3 to 8.3 μm in spring steel[13]. Structural parts made of ULC automotive steel are prone to fatigue damage due to cyclic loading. Currently, the fatigue performance of bearing and spring steel has been reported largely[14-16]. Hu et al. reported that as the basicity of refining slag increased from 3.4 to 5.0, the fatigue life of spring steel increased from 3.5×10^4 to 7.8×10^6 cycles[17]. However, few reports focusing on the fatigue properties of ULC automotive steel have been available so far.

In this work, a plant trial of Al-killed ULC automotive steel was performed with five different Al_2O_3 contents in refining slags, and the influence of Al_2O_3 content in refining slag on cleanliness and fatigue property of ULC automotive steel have been investigated. The size, distribution, morphology and chemical compositions of inclusions were measured and analyzed. The inclusion-adsorption capacity of the refining slag has been calculated by using thermodynamic software. The fatigue life of ULC automotive steel was found from $1.4x10^4$ down to $0.9x10^4$ cycles at a stress amplitude of 400 MPa.

2. Experimental

The experiment was carried out in a domestic factory that producing ULC automotive steel. The production of ULC automotive steel undergoes via the process of basic oxygen furnace (BOF)→ladle furnace refining (LF)→Ruhrstahl Heraeus degassing (RH)→continuous casting (CC), and the volume of the experimental ladle is 110 t. Five groups of refining slag samples were analyzed and their adsorption capacity for inclusions were calculated. The extraction procedure of inclusions using electrolysis, anhydrous methanol was used as electrolyte. The polished sample was hung in a sleeve as the anode, and the outer cast iron sleeve was used as the

*e-mail: duxy@lut.cn

cathode. The samples were electrolyzed for 72 hours under a 6 A current, and a filter was placed in the middle to collect the anode slime. The anode slime was subjected to magnetic separation and washing to separate the inclusions, carbides, and iron oxides. After reduction and magnetic treatment, the inclusions were obtained. The schematic of the electrolysis devices and inclusion extraction process were given in Figure 1.The number, size, and morphology of inclusions were analyzed through the scanning electron microscopy (SEM) and INCASteel automatic inclusion analyzer.

In the production of Al-killed ULC automotive steel, accompanying the slag making, arc heating and argon stirring in the process of LF refining. The aims of the LF refining process are desulfuration, deoxygenation, arc heating and inclusion removal. The Al_2O_3 contents in the slag were adjusted during slag-making process in LF refining. LF refining process and sampling time are given in Figure 2. In this process, the static blowing time is 8-10 min, and the rates of Ar gas about static blowing and strong stirring were controlled in the range of 40-60 Nm^3/h and 800-1000 Nm^3/h, respectively. After LF refining, the ladle was transported to the RH station for degassing with the vacuum of 2.0 mbar for 15-30 min. Finally, the ULC automotive steel was obtained after undergoing CC and rolling.

The slag samples were taken from the initial state and the end of LF process, the steel samples were taken from the end of LF process, as shown in Figure 2. The steel samples were extracted by pail samplers, racket samplers and acicular samplers at the position of 300 mm below the slag surface, as shown in Figure 3. The slag samples were obtained by

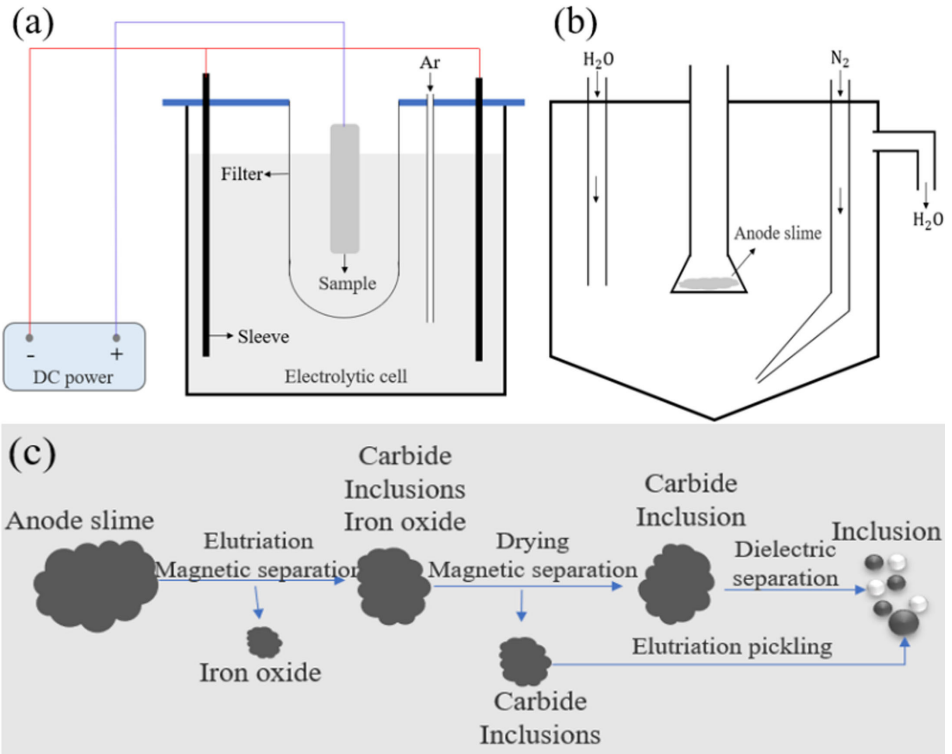

Figure 1. Schematic of electrolysis devices and inclusion extraction process (a: Schematic of electrolysis devices; b: Schematic of elutriation devices; c: Extraction process of inclusions).

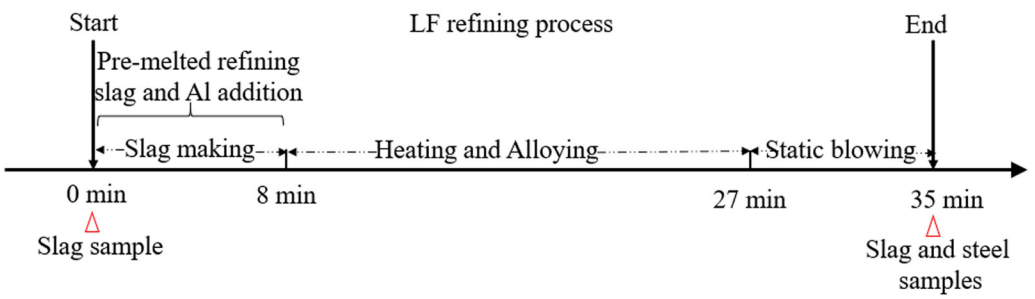

Figure 2. The sketch diagram of LF refining process and sampling time of Al-killed ULC automotive steel.

sampling stick, then, they were prepared in the form of tablet pressing. Slag samples were measured by Panaco Epsilon 3X EDXRF spectrometer, after calibration with the standard sample, the mass fractions of components in the slag samples were obtained. The pail samples were analyzed with the INCASteel automatic inclusions analysis system and the acicular samples were analyzed for the T.O content with the LECO-ON83 oxygen-nitrogen analyzer. The chemical components of steel samples were measured with the OBLF QSG750-II direct-reading spectrometer. The steel samples were subjected to test their fatigue properties at a rotating frequency of 500 Hz.

3. Results and Discussion

3.1. Results

The chemical compositions of the slag samples before and after LF refining are listed in Table 1 and Table 2, the chemical compositions of steel samples are listed in Table 3, respectively. Table 1 contains six main components and alkalinity of the refining slag, which can be seen that TFe content is very high while the Al_2O_3 content is low. The total compositions of slag in Table 1 are less than 100%, mainly because there are small amounts of

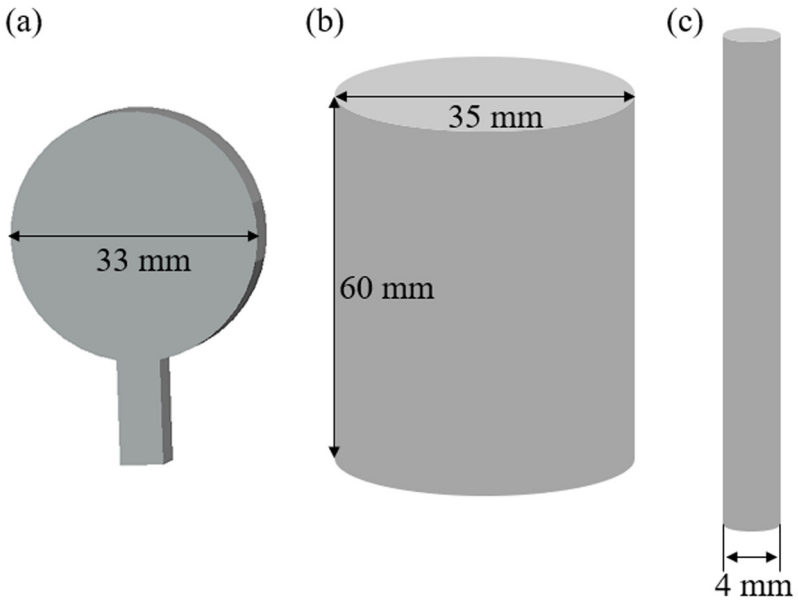

Figure 3. Steel samples taken from the end of LF process of ULC automotive steel; (a) racket sampler; (b) pail sampler; (c) acicular sampler.

Table 1. The chemical compositions of slag samples before LF (mass%).

Sample Nr.	TFe	MnO	CaO	SiO_2	Al_2O_3	MgO	R_2(CaO/ SiO_2)	CaO/Al_2O_3
1	18.22	3.35	45.13	13.71	1.27	8.31	3.29	35.54
2	20.36	3.93	44.36	12.47	1.39	8.74	3.56	31.91
3	19.6	2.71	46.5	12.52	1.3	10.07	3.72	35.77
4	21.65	2.63	41.68	13.56	1.58	9.7	3.07	26.38
5	18.78	2.71	47.57	13.11	1.11	8.89	3.63	42.86

Table 2. The chemical compositions of slag samples of LF end (mass%).

Sample Nr.	TFe	MnO	CaO	SiO_2	Al_2O_3	MgO	R_2(CaO/ SiO_2)	CaO/Al_2O_3
6	0.39	0.148	57.05	5.08	19.92	8.8	11.23	2.86
7	0.33	0.172	53.86	6.56	24.86	8.22	8.21	2.17
8	0.35	0.191	52.39	6.96	30.08	6.86	7.53	1.74
9	0.46	0.065	50.34	7.29	34.86	6.79	6.91	1.44
10	0.39	0.097	45.58	7.89	39.73	6.17	5.78	1.15

P_2O_5, Cr_2O_3, S and other components in refining slag. Moreover, the $R_2(CaO/SiO_2)$ of the ULC automotive steel is between 3.07 and 3.72, which is not only beneficial to protect the furnace lining and prolong the service life of the furnace body, but also plays an important role in regulating the FeO content in steel slag. The Al_2O_3 content was controlled by the pre-melted refining slag at different numerical value, the resulting compositions of the refining slag were detailed in Table 2, revealing slight variations in chemical compositions between the five samples except Al_2O_3 and CaO contents. Table 4 details the T.O content of the five steel samples from the end of LF process, which can see that the T.O content is increasing. The inclusions were mainly counted that containing Al_2O_3 in Table 5, with the increase of Al_2O_3 content in refining slag, the maximum size of the inclusions increased.

The schematic diagram of the Al_2O_3 content in refining slag, the T.O content and number density of inclusions in molten steel were shown in Figure 4. The T.O content and number density of inclusions were observed to increase with the Al_2O_3 content increasing as shown in Figure 5 and Figure 6. The information of non-metal inclusions in ULC steels were given in Table 5 and Table 6, the inclusions' size distribution was shown in Figure 7. Study has verified that when the number density of non-metal inclusions at 5.2-6.6 per mm^2, the inclusions that containing Al_2O_3 increased by about 5% at 5 - 10 μm, it harmed the cleanliness and anti-fatigue properties of aluminum deoxidized steel[13]. The number density of non-metal inclusions were 5.22-9.06 per mm^2 in samples 2-5 in Table 5, therefore, it can be deduced that the proportion of inclusions greater than 10 μm increased by 5%, which seriously harmed the cleanliness and anti-fatigue performance of the ULC automotive steel.

The morphology and composition of the inclusions were analyzed by scanning electron microscope and energy spectrum in Figure 8. The inclusions are mainly yellow and white transparent inclusions with large particle size, yellow and black opaque inclusions, and some small spherical inclusions like Figure 8(a), Figure 8 (b) shows that the main ingredient of spherical morphologies inclusion was Al_2O_3 observed by scanning electron microscopy-energy disperse spectroscopy (SEM-EDS). In addition, an analysis of inclusion clusters larger than 40 μm in Figure 8(c) found Al_2O_3 to be a major constituent component.

Table 3. The chemical compositions of the steel samples at the end of LF process /%.

Sample	C	Mn	S	P	Si	Als	N	Ti
1	0.031	0.042	0.007	0.01	0.003	0.001	0.002	0.00
2	0.023	0.041	0.005	0.01	0.003	0.003	0.0019	0.00
3	0.024	0.038	0.006	0.011	0.003	0.001	0.0025	0.00
4	0.025	0.035	0.006	0.01	0.002	0.002	0.0021	0.00
5	0.023	0.036	0.006	0.008	0.003	0.001	0.0023	0.00

Table 4. The T.O content of the five steel samples at the end of LF process (ppm).

Sample Nr.	1	2	3	4	5
T.O/ppm	12	13	15	17	18

Table 5. Inclusion analysis of the samples 1 to 5 with INCASteel automatic inclusion analyzer.

Sample Nr.	scanning area/mm^2	Inclusion number	maximum size/um	minimum size/um	number density #/mm^2
1	50.81	207	13.83	1.08	4.07
2	53.06	277	15.2	1.05	5.22
3	51.5	267	16.82	1.08	5.18
4	55.14	336	21.2	1.05	6.09
5	52.54	476	45.49	1.05	9.06

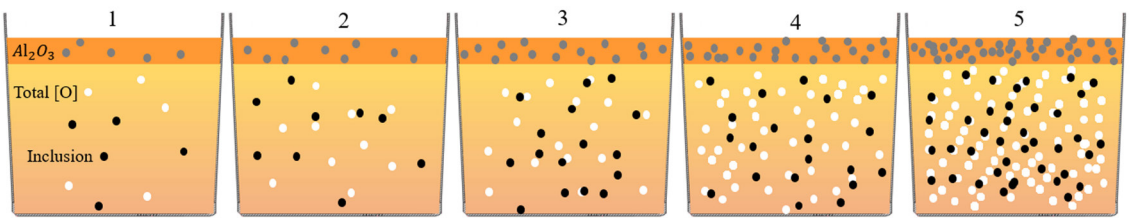

Figure 4. The schematic between the Al_2O_3 content in refining slag, the T.O content and number density of inclusions in molten steel of Al-killed ULC automotive steel.

Table 6. Inclusions types of different sizes.

Sample Nr.	Sizes/um	Main types of inclusions
1	2-4	Small spherical Al_2O_3
	4-10	Spherical Al_2O_3
	>10	——
2	2-4	Small spherical Al_2O_3
	4-10	Spherical Al_2O_3
	>10	Al_2O_3· CaO cluster + Al_2O_3 cluster
3	2-4	Small spherical Al_2O_3
	4-10	Al_2O_3 cluster + spherical Al_2O_3
	>10	Al_2O_3·CaO·SiO_2 cluster + Al_2O_3 cluster
4	2-4	Small spherical Al_2O_3
	4-10	Al_2O_3 cluster + spherical Al_2O_3
	>10	Al_2O_3·CaO·SiO_2cluster + Al_2O_3cluster + spherical Al_2O_3
5	2-4	Small spherical Al_2O_3
	4-10	Al_2O_3 cluster + spherical Al_2O_3
	>10	Al_2O_3·CaO·SiO_2 cluster + Al_2O_3cluster + large spherical Al_2O_3

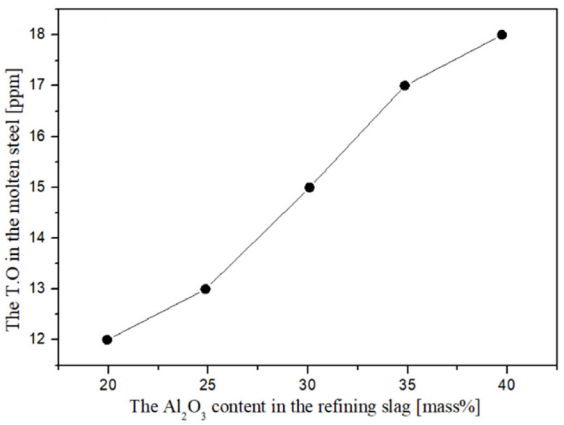

Figure 5. The relationship between Al_2O_3 in refining slag and T.O in ULC automotive steel.

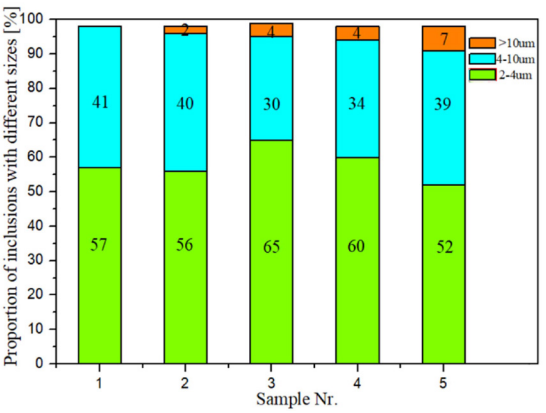

Figure 7. Proportion of inclusions of different sizes in ULC automotive steel.

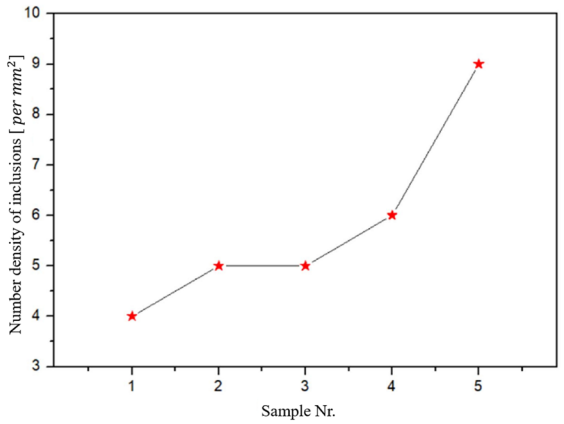

Figure 6. Number density of inclusions in ULC automotive steel.

4. Discussion

It is well established that reactions between slag and molten steel take place constantly, due to the huge contact area that provides good kinetic conditions. Thus, the slag, steel and inclusions can all react with each other, which enables inclusion removal and modification. To investigate the relationship between the three, the inclusions in steel were assumed to consist only of metal oxides during the refining process, and the resulting chemical reaction in molten steel is given as follows:

$$x[M] + y[O] = \left(M_xO_y\right)_{slag} \quad (1)$$

where M represents the metal atom in steel and the [O] represents the dissolved oxygen. $(M_xO_y)_{slag}$ represents

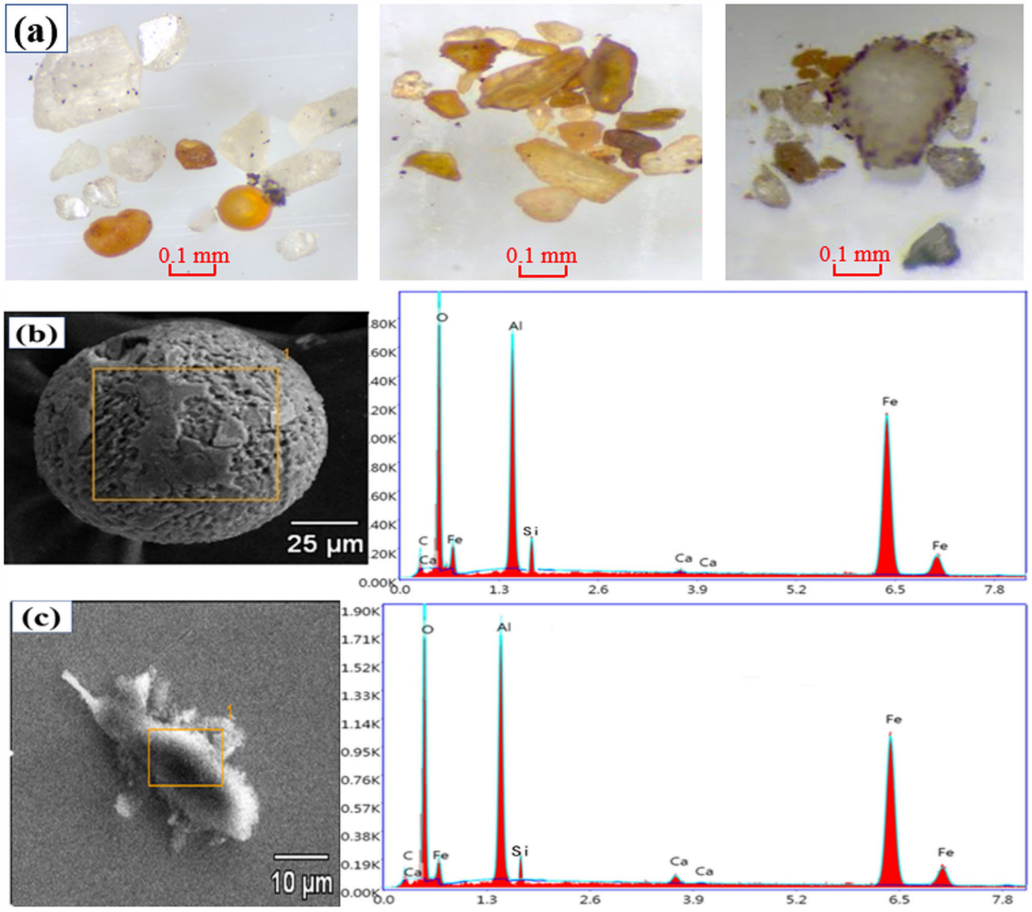

Figure 8. Scanning electron microscopy-energy disperse spectroscopy of inclusions; (a) Morphology of inclusions;(b) Spherical morphologies Al_2O_3 inclusion and EDS; (c) Clusters Al_2O_3 inclusion and EDS.

contents of MgO, Al_2O_3, CaO, etc. in the slag. During the refining process, M_xO_y floats up to steel slag, and the Gibbs free energy is expressed as:

$$\Delta G_{slag/steel} = \Delta G^{\theta}_{slag/steel} + RTln\frac{a_{(MxOy)_{slag}}}{a^x_{[M]}a^y_{[O]}} \quad (2)$$

When the reaction reaches equilibrium, $\Delta G_{slag/steel} = 0$, and the standard Gibbs free energy can be written as:

$$\Delta G^{\theta}_{slag/steel} = -RTln\frac{a_{(MxOy)_{slag}}}{a^x_{[M]}a^y_{[O]}} \quad (3)$$

Furthermore, inclusions are produced in steel during the refining process via the following chemical reaction:

$$x[\mathrm{Me}] + y[\mathrm{O}] = \left(\mathrm{Me_xO_y}\right)_{\mathrm{inclusion}} \quad (4)$$

where [Me] represents the metal atom in steel, [O] represents the dissolved oxygen, and (Me_xO_y) represents the inclusions in steel. Subsequently, the Gibbs free energy of inclusion formation can be expressed as follows:

$$\Delta G_{inclusion/steel} = \Delta G^{\theta}_{inclusion/steel} + RTln\frac{a_{(MexOy)_{inclusion}}}{a^x_{[Me]}a^y_{[O]}} \quad (5)$$

When the reaction reaches equilibrium, $\Delta G_{inclusion/steel} = 0$, and the standard Gibbs free energy can be obtained by the following equation:

$$\Delta G^{\theta}_{inclusion/steel} = -RTln\frac{a_{(MexOy)_{inclusion}}}{a^x_{[Me]}a^y_{[O]}} \quad (6)$$

The metal atoms in steel are represented by [M] and [Me], where [M]=[Me]. As such, if the same activity standard is adopted to both the inclusions and slag, their standard Gibbs free energies should be equivalent[18]. Therefore, by combining equations (3) and (6), equations (7) and (8) can be obtained as follows:

$$\Delta G^{o}_{slag/steel} \Rightarrow \Delta G^{o}_{inclusion/steel} \quad (7)$$

$$a_{(MxOy)_{slag}} \Rightarrow a_{(MexOy)_{inclusion}} \quad (8)$$

From the equation (8), it is evident that the inclusions have a similar composition to the slag, and the composition changes of inclusions are consistent with those of the slag in the refining process. Thus, as the Al_2O_3 content in refining slag increased, the amount of Al_2O_3 inclusions in the molten steel should also increase, which is consistent with the statistical results in Table 5.

At the preliminary stage of deoxidation, most of the inclusions were composed of Al_2O_3. However, as the reaction progresses, the [Mg] in the molten steel will react with Al_2O_3 inclusions via the reaction in equation (9)[19]. The addition of aluminum results in a reaction with CaO and SiO_2 within the slag, which can lead to an increase of [Ca] and [Si] in the steel, as given by equation (10) and (11).

$$[Mg]+[O]+(Al_2O_3)_{inclusion}=(MgO\cdot Al_2O_3)_{inclusion} \quad (9)$$

$$2[Al]+3(CaO)_{slag}=3[Ca]+(Al_2O_3)_{slag} \quad (10)$$

$$4[Al]+3(SiO_2)_{slag}=3[Si]+2(Al_2O_3)_{slag} \quad (11)$$

The increase of [Ca] and [Si] content in the steel converts the ($MgO\cdot Al_2O_3$) inclusions to $CaO\cdot MgO\cdot SiO_2\cdot Al_2O_3$ inclusions, given by the reaction in equation (12).

$$x[Ca]+y[Si]+(zMgO\cdot mAl_2O_3)_{inclusion}= (xCaO\cdot(z-2y-x)MgO\cdot ySiO_2\cdot mAl_2O_3)+(x+2y)[Mg] \quad (12)$$

The conversion from Al_2O_3 inclusion to $CaO\cdot MgO\cdot SiO_2\cdot Al_2O_3$ inclusion in the refining process has been investigated in previous work[20]. The $CaO\cdot MgO\cdot SiO_2\cdot Al_2O_3$ inclusions have a relatively low melting point and exist in liquid at steel-making temperature. Besides, the wettability of MgO inclusions in molten steel is poor, and agglomeration occurs hardly[21], while Al_2O_3 inclusions have a strong tendency to agglomerate[22]. As the refining process continues, the major components of inclusions are Al_2O_3 in the later refining period, which leading Al_2O_3 inclusions to form clusters[23], and cluster inclusions contain a small amount of CaO and SiO_2, as illustrated in Figure 8(c).

The inclusion-adsorption capacity of the refining slag can be given as follow[24]:

$$K^{\Theta}=\rho_{slag}^{\frac{1}{3}}\left(\frac{k_BT}{6\pi a_0}\right)^{2/3}\left(\frac{\eta_{slag}}{\rho_{slag}}\right)^{-5/6}\frac{X_{Al_2O_3}^{slag}-X_{Al_2O_3}^{interface}}{X_{Al_2O_3}^{interface}-100} \quad (13)$$

Where ρ_{slag} represents the density of slag, $kg\cdot m^{-3}$, k_B represents the Boltzmann constant, $k_B=1.3806\times10^{-23}J\cdot K^{-1}$, T represents the slag temperature, T=1873k, a_0 represents the radius of the diffusion unit of aluminum oxygen anion group, and it sets as 2.0×10^{-10} m[24]. η_{slag} represents Kinetic viscosity of slag, Pa·s, $X_{Al_2O_3}^{slag}$ represents the mass percentage of Al_2O_3 in slag, wt%, $X_{Al_2O_3}^{interface}$ represents the saturated Al_2O_3 concentration in the slag system, which can be calculated by the balance module of FactSage thermodynamic calculation software. K^{Θ} represents the inclusion-adsorption capacity of refining slag to Al_2O_3 inclusion. The adsorption rate of Al_2O_3 inclusions in molten steel by molten slag is different from that of alumina cylinder in molten slag under experimental conditions. However, under similar slag conditions, the value of K^{Θ} can be used to represent the relative rate of alumina inclusion-adsorption by refining slag[24].

From the equation (13), the increase of Al_2O_3 content in the slag leading to a subsequent decrease in the adsorption capacity for Al_2O_3 inclusions, curves of equal inclusion-adsorption capacity of refining slag for inclusions are shown in Figure 9. As illustrated by the thermodynamic computational analysis with FactSage in Figure 9, the inclusion-adsorption capacity of the refining slag for samples 6 to 10 in Table 2 are 210.30, 157.90, 90.34, 79.40 and 57.12, respectively. There is a large fluctuation of CaO content besides Al_2O_3 in Table 2, study has shown that when the CaO content in the refining slag was between 48-66%, it had little effect on the adsorption of Al_2O_3 inclusions[25]. In Table 2, the CaO content in the refining slag was 45.58-57.05%, it was feasible to use K^{Θ} to express the adsorption capacity of inclusions in the refining slag. With the increase of Al_2O_3 content in the refining slag, the inclusion-adsorption capacity decreases sharply.

The analyses above are consistent with the results in Figure 6 and Table 5, where the number density of inclusions is observed increasing from 4 per mm^2 to 9 per mm^2 as the Al_2O_3 content increased in the refining slag.

Fatigue behavior is an important mechanical property for many kinds of materials, especially in the automotive industry, and most of the fatigue fractures originate from internal or surface inclusions. Previous studies have proved that clusters of Al_2O_3 particles cause poor fatigue properties in structural steel[26,27], and oxide inclusions were most likely to cause fatigue fracture[28,29]. As fatigue life is an important mechanical performance index, the fatigue property of the five steel samples were investigated at 400 MPa stress amplitude. The shape and size of specimens are shown in Figure 10. These results are shown in Figure 11, indicating the fatigue life decreases with the increase of Al_2O_3 content in the refining slag. By analyzing the fatigue fracture, it is found that there is Al_2O_3 in the crack as shown in Figure 12.

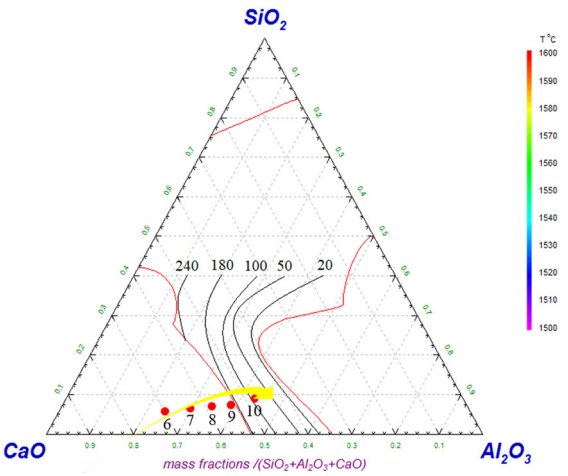

Figure 9. Inclusion-adsorption capacity of refining slag with different Al_2O_3 contents in ULC automotive steel.

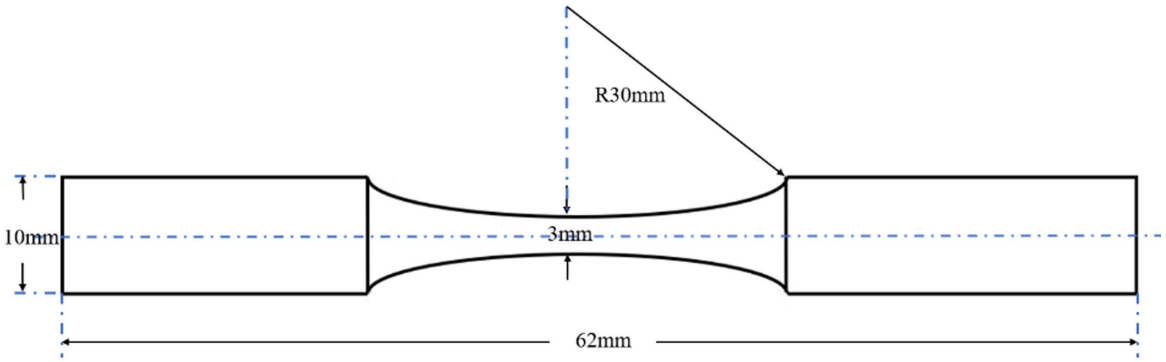

Figure 10. Shape and size of a specimen for fatigue test.

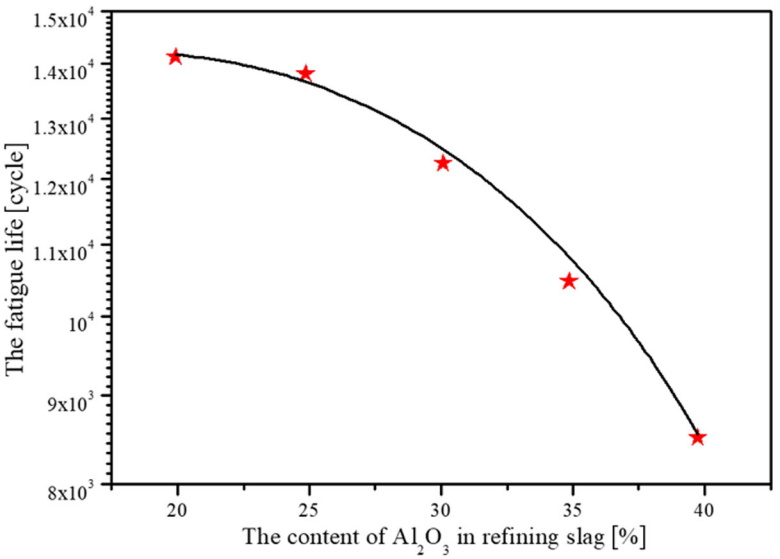

Figure 11. The relationship between Al_2O_3 content in slag and fatigue life of ULC automotive steel.

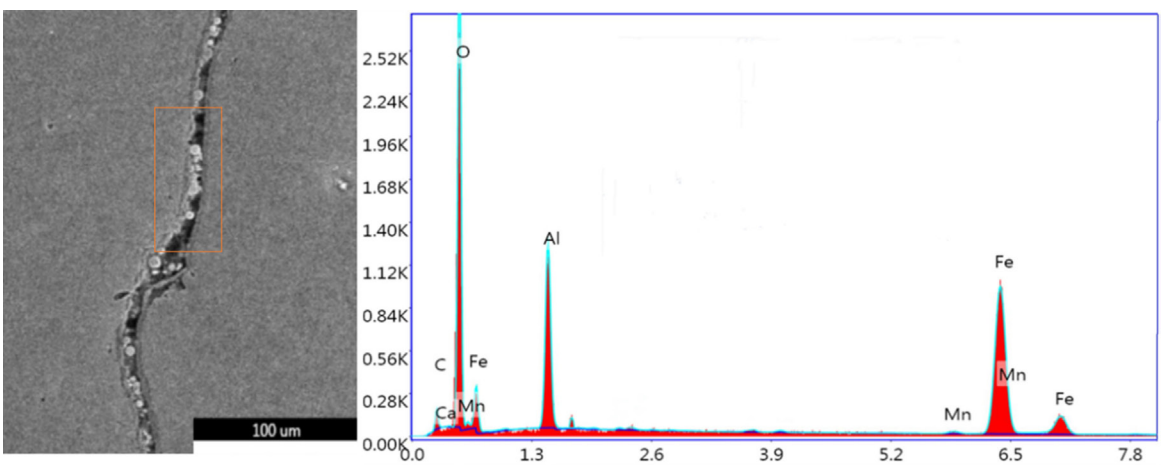

Figure 12. Scanning electron microscopy-energy disperse spectroscopy of crack.

When the Al_2O_3 content increased from 19.92% to 39.73% in refining slag, the fatigue life was observed decreasing from $1.4x10^4$ to $0.85x10^4$ cycles as shown in Figure 11. The relationship between Al_2O_3 content in the refining slag and fatigue life of steel is expressed in equation (14), it can help to predict the fatigue property of ULC automotive steel.

$$Y = -9.31X^2 + 292.26X + 1.2*10^4 \quad (14)$$

where Y represents the fatigue life and X represents the Al_2O_3 content (%) in refining slag.

5. Conclusion

This study aimed at investigating the relationship between Al_2O_3 content in refining slag and the cleanliness and mechanical properties of ULC automotive steel. By analyzing the fatigue property and statistically evaluating the inclusions in ULC automotive steel, the main conclusions may be drawn as follows:

1. With the increase of Al_2O_3 content from 19.92% to 39.73% in refining slag, the T.O content and inclusion number density in steel increase from 12 to 18 ppm and 4 to 9 per mm^2, respectively, the inclusion-adsorption capacity of refining slag from 210.30 down to 57.12.
2. The conversion of inclusion compositions from Al_2O_3 to $CaO{\cdot}MgO{\cdot}SiO_2{\cdot}Al_2O_3$ in the refining process. With the increase of Al_2O_3 content in refining slag, the proportion of inclusions which sizes larger than 10μm rose from 0% to 7% due to the aggregation of inclusions in molten steel.
3. When the Al_2O_3 content in refining slag increased from 19.92% to 39.73%, the fatigue life reduced from $1.4x10^4$ to $0.9x10^4$ cycles, and an expression for the fitted of this relationship was obtained to predict the fatigue property of ULC automotive steel.

6. Acknowledgements

This work was supported by State Key Laboratory of Advanced Processing and Recycling of Non-Ferrous Metals in Lanzhou University of Technology.

7. References

1. Wang XH. Non-metallic inclusion control technology for high quality cold rolled steel sheets. Iron Steel. 2013;48(9):1-9.
2. Wang R, Bao YP, Yan ZJ, Li DZ, Kang Y. Comparison between the surface defects caused by Al_2O_3 and TiN inclusions in interstitial-free steel auto sheets. Int J Miner Metall Mater. 2019;26(2):178-85.
3. Liu XG, Wang C, Gui JT, Xiao QQ, Guo BF. Effect of MnS inclusions on deformation behavior of matrix based on in-situ experiment. Mater Sci Eng A. 2019;746:239-47.
4. Cao ZX, Shi ZY, Yu F, Gao WQ, Wen YQ. A new proposed Weibull distribution of inclusion size and its correlation with rolling contact fatigue life of an extra clean bearing steel. Int J Fatigue. 2019;126:1-5.
5. Li HB, Yuan P, Bin C, Liu FG. The influence of slag chemistry on the formation of sliver defects. Ironmak Steelmak. 2019;46(5):463-8.
6. Gu C, Bao YP, Gan P, Lian JH, Münstermann S. An experimental study on the impact of deoxidation methods on the fatigue properties of bearing steels. Steel Res Int. 2018;89(9):1800129.
7. Gu C, Lian JH, Bao YP, Xiao W, Munstermann S. Numerical study of the effect of inclusions on the residual stress distribution in high-strength martensitic steels during cooling. Appl Sci (Basel). 2019;9(3):455.
8. Banerjee A, Prusty BG. Fatigue and fracture behaviour of austenitic-martensitic high carbon steel under high cycle fatigue: an experimental investigation. Mater Sci Eng A. 2019;749:79-88.
9. Guo JL, Bao YP, Wang M. Cleanliness of Ti-bearing Al-killed ultra-low-carbon steel during different heating processes. Int J Miner Metall Mater. 2017;24(12):1370-8.
10. Yang W, Wang XH, Zhang LF, Shan QL, Liu XF. Cleanliness of low carbon aluminum-killed steels during secondary refining processes. Steel Res Int. 2013;84(5):473-89.
11. Park JS, Park JH. Effect of slag composition on the concentration of Al_2O_3 in the inclusions in Si-Mn-killed steel. Metall Mater Trans, B, Process Metall Mater Proc Sci. 2014;45(3):953-60.
12. Pereira JAM, da Rocha VC, Yoshioka A, Bielefeldt WV, Vilela ACF. Analysis of secondary refining slag parameters with focus on inclusion cleanliness. Mater Res. 2018;21(5):e20180296.
13. Hu YH, Chen WQ. Influence of refining slag composition on cleanness and fatigue life of 60Si2MnA spring steel. Ironmak Steelmak. 2016;43(5):340-50.
14. Gu C, Wang M, Bao YP, Wang FM, Lian JH. Quantitative analysis of inclusion engineering on the fatigue property improvement of bearing steel. Metals (Basel). 2019;9(476):1-15.
15. Hu Y, Chen WQ, Wan CJ, Wang FJ, Han HB. Effect of deoxidation process on inclusion and fatigue performance of spring steel for automobile suspension. Metall Mater Trans, B, Process Metall Mater Proc Sci. 2018;49:569-80.
16. Zerbst U, Madia M, Klinger C, Bettge D, Murakami Y. Defects as a root cause of fatigue failure of metallic components. II: non-metallic inclusions. Eng Fail Anal. 2019;98:228-39.
17. Hu Y, Chen WQ, Han HB, Bai RJ. Influence of calcium treatment on cleanness and fatigue life of 60Si2MnA spring steel. Ironmak Steelmak. 2017;44(1):28-35.
18. Wang XH, Jiang M, Chen P, Li HB. Study on formation of non-metallic inclusions with lower melting temperatures in extra low oxygen special steels. Sci China Technol Sci. 2012;55(7):1863-72.
19. Ji YQ, Liu CY, Lu Y. Effects of FeO and CaO/Al_2O_3 ratio in slag on the cleanliness of Al-killed steel. Metall Mater Trans, B, Process Metall Mater Proc Sci. 2018;49(6):3127-36.
20. Yoshioka T, Ideguchi T, Karasev A, Ohba Y, Jonsson PG. The effect of a high Al content on the variation of the total oxygen content in the steel melt during a secondary refining process. Steel Res Int. 2018;89(2):1-9.
21. Hong L, Sun Q, Lv K, Kei K, Hao Y, Wei K. Study on application of Mg alloy in the steelmaking process. Shanghai metals. 2015;37(6):69-72.
22. Xiao PC. Evolution of hook-like shell and its effect on surface cleanness of IF steel slab [Ph.D. Thesis]. Tangshan: North China University of Science and Technology; 2018.
23. Mu WZ, Dogan N, Coley KS. In situ observation of deformation behavior of chain aggregate inclusions: a case study for Al_2O_3 at a liquid steel/argon interface. J Min Sci. 2018;53(18):13203-15.
24. Guo YT. Study on refining process optimization and sulfide morphology for resulfurized free-cutting structural steel [Ph.D. Thesis]. Chongqing: College of Materials Science and Engineering of Chongqing University; 2017.
25. Rocabois P, Lehmann J, Gatellier C. Non-metallic inclusion entrapment by slag: laboratory investigation. Ironmak Steelmak. 2003;30(2):95-100.

26. Yang CY, Luan YK, Li DZ, Li YY. Very high cycle fatigue properties of bearing steel with different aluminum and sulfur content. Int J Fatigue. 2018;116:396-408.
27. Karr U, Schönbauer B, Fitzka M, Tamura E, Sandaiji Y, Murakami S, et al. Inclusion initiated fracture under cyclic torsion very high cycle fatigue at different load ratio. Int J Fatigue. 2019;122:199-207.
28. Li ZD, Zhou ST, Yang CF, Yong QL. High/very high cycle fatigue behaviors of medium carbon pearlitic wheel steels and the effects of microstructure and non-metallic inclusions. Mater Sci Eng A. 2019;764:138-208.
29. Liu JP, Zhou QY, Zhang YH, Liu FS, Tian CH, Li C, et al. The formation of martensite during the propagation of fatigue cracks in pearlitic rail steel. Mater Sci Eng A. 2019;747:199-205.